Analysing the Influence of Geometry and Pressure on Corona Discharges

Jordi-Roger Riba[1], Pau Bas-Calopa[1] and Manuel Moreno-Eguilaz[1]

[1] Universitat Politècnica de Catalunya, Terrassa, Spain

E-mail: jordi.riba-ruiz@upc.edu

Received xxxxxx
Accepted for publication xxxxxx
Published xxxxxx

Abstract

In this work, the authors propose an experiment aimed for undergraduate laboratories with the aim of introducing different novelties as a topic for practical sessions or student projects. The topics here investigated are appropriate for students with intermediate physics knowledge. Corona discharges are little studied in regular physics courses despite their practical importance in different areas, such as the distribution and transmission of electrical power, generation of ozone, particulate removal in air conditioning systems, improvement of wettability in polymeric materials, or the removal of electrostatic charges from the surface of airplanes among others. This work analyses the minimum voltage level leading to corona discharges and the influence of geometry and atmospheric pressure because these two factors are the most influential to determine the minimum voltage at which corona discharges appear.
.

Keywords: corona discharges, ionization, high-voltage, low pressure

1. Introduction

To maximize efficiency and reduce operational costs, power transmission lines operate at very high-voltage levels. However, raising the voltage significantly increase the risk of electrical discharges, and in particular of corona activity, which have harmful effects on transmission lines. However, corona discharges are deliberately produced in various industrial processes such as the production of ozone in water treatment plants, the removal of particles in air conditioning systems or the improvement of the surface of polymeric materials. Corona activity can be controlled by adjusting the electric field strength on the surface of the high-voltage electrodes [1], because electrical discharges are triggered by the electric field strength.

In uniform electric fields as those generated between two parallel plates separated by atmospheric air, when the voltage between the two plates (electrodes) increases steadily, it will inevitably lead to a complete breakdown of the air gap. However, in the case of non-uniform electric fields, a gradual voltage increase first leads to partial discharges [2] and if the voltage is further increased, finally a complete breakdown of the gap will be produced. Corona is a type of partial discharge occurring in air (or a gas medium), i.e., a self-sustained luminous discharge that produces a conductive area around the electrode but it does not completely bridge the air gap between the two electrodes. When the maximum electric field intensity at the surface of conductor exceeds a certain value [3,4], corona initiates in a limited region surrounding the high-voltage electrode because air molecules become ionized [5] due to the impact of free electrons, hence developing an electron avalanche process [6]. Two regions can be distinguished within the air gap between the two metallic electrodes, i.e., the ionization and the low-field regions. The first one, with a usual size of several millimetres, is the area closest to the high-voltage electrode, having an intense electric field that sustains the ionization process. The low-field or drift region fills the inter-electrode

space, so it comprises the region between the limit of the ionization area and the collecting electrode. The electric field in the low-field region cannot sustain the ionization process [7], so it stabilizes corona activity [8].

Positive and negative coronas reveal different voltage-current patterns, which is essentially due to the mass difference between electrons and positive ions [9]. However, a physical description of the phenomenon is complex due to the ionization process and the chemical reactions occurring within the gas during the discharge process [10]. In power systems, corona discharges must be avoided, because they produce negative effects, and reduce their performance due to the power losses and generation of chemical by-products, such as ozone and nitrogen oxides among others [11]. The corona activity produces acoustic and electromagnetic emissions, including ultraviolet and visible light, and radio interference noise. Since most of the radiation produced by corona activity falls within the UV spectrum, it is almost invisible in daylight. Due of the complexity of the phenomenon, there are no theoretical formulas to determine the critical electric field at which corona initiates, so that for a given geometry, the conditions leading to corona are usually determined from experimental data.

Several variables influence the onset of corona, such as the type of voltage applied (direct current or alternating current, low or high frequency), geometry, surface state, or weather conditions (air temperature, pressure, density, pressure, humidity or pollution). Apart of the applied voltage level, geometry and atmospheric pressure play a leading role.

It is well known that the electric field near a sharp edge of a conductor is higher, so the electric field lines are more closely spaced nearer the conductor compared to a flat conductor. Therefore, electrical discharges are more likely to occur in areas of the electrode surface with smaller radius.

The dielectric strength of air is greatly reduced with pressure [12–14], so at high altitude (lower pressure), lower voltages are required to initiate corona discharges compared to sea level. Electrical installations in the Andes or the Himalayas, where altitudes between 4500 and 5300 m are possible and need special attention, because at 5000 m the pressure is reduced by about 45% compared to that at sea level. Similar or even stronger effects occur in electrical installations found in aircrafts, because most commercial jetliners have a service ceiling of about 42000 ft (12.8 km), so electronic and electrical systems found in unpressured compartments must withstand pressures in the 17 – 101 kPa range.

Because of the multiphysics origin and the complexity of corona discharges, there are no theoretical-based analytical formulas to describe the conditions at which corona discharges initiate. This paper presents a method for determining the effect of geometry and atmospheric pressure on the minimum voltage at which corona discharges can develop. Although spherical electrodes are discussed, the method applied here can be generalized to other types of electrodes. The approach proposed in this paper can be applied to develop a project or a laboratory practical for undergraduate courses. Regardless of the importance and practical impact of corona discharges on electrical systems, this topic is infrequently studied in regular courses, so to overcome this problem, this work proposes a students' project or practical session to analyse this subject from an experimental point of view.

This paper is organized as follows. Section 2 explains two of the most influential factors affecting corona discharges, i.e., geometry and air pressure. Section 3 develops the experimental procedure to find the corona extinction voltage. Section 4 details the analysed electrodes and the experimental setup used in the experiments. Section 5 presents and discusses the experimental results. Finally, Section 6 summarizes the conclusions of this work.

2. Factors influencing corona discharges

This section briefly discusses two of the most influential factors affecting corona discharges, i.e., geometry and atmospheric pressure.

2.1 Effect of geometry on corona discharges

As explained, geometry and specifically the curvature radius play a key role to determine the minimum voltage level at which corona activity can be detected, which is known as the corona extinction voltage (CEV).

This paper studies spherical electrodes to analyse the effect of the geometry on the CEV value, as they are low-cost (steel bearing balls are used), have a definite and regular radius and a uniform surface finish. As the electric field near a sharp conductor is known to be higher, it is expected that when dealing with small radius spheres, corona activity will start at lower CEV values compared to those expected in larger spheres.

Fig. 1 shows the electric field distribution generated by two sphere-plane electrodes with different sphere radii under the same conditions (applied voltage and sphere-plane separation).

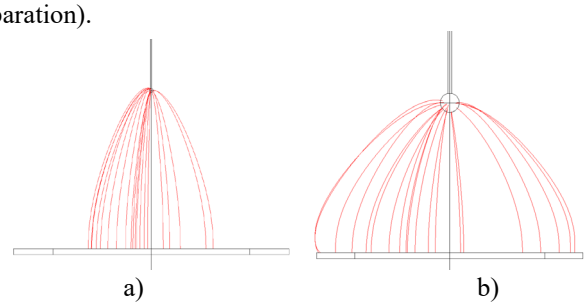

Fig. 1. a) Electric field lines on the surface of a spherical electrode of radius 1 mm placed 80 mm above a ground plane. b) Electric field lines on the surface of a spherical electrode of radius 5 mm placed 80 mm above a ground plane.

Fig. 1 shows that the electric field strength at the surface points of the largest sphere is lower than that of the smaller spherical electrode. It can be seen by the lower density of electric field lines on its surface.

2.2. EFFECT OF PRESSURE ON CORONA DISCHARGES

Table 1 shows the standardized relationships among air temperature, pressure and density according to the U.S. standard atmosphere [15].

Table 1. Relationships among altitude, pressure and air density according to the U.S. standard atmosphere [15].

Altitude (m)	Temperature (ºC)	Pressure (kPa)	Air density (kg/m^3)	Relative air density (-)
0	15.0	101.325	1.225	1.000
1000	8.5	89.875	1.112	0.907
2000	2.0	79.495	1.006	0.822
3000	-4.5	70.109	0.909	0.742
4000	-11.0	61.640	0.819	0.669
5000	-17.5	54.020	0.736	0.601
6000	-14.0	47.181	0.660	0.539
7000	-30.5	41.061	0.590	0.481
8000	-37.0	35.600	0.525	0.429
9000	-43.5	30.742	0.466	0.381
10000	-50.0	26.436	0.412	0.337
11000	-56.5	22.632	0.364	0.297
12000	-56.5	19.330	0.311	0.254

Pressure has a deep influence on the minimum voltage level at which corona discharges initiate, so in view of the values in Table 1, this paper will consider the pressure range between 100 kPa and 20 kPa to cover the 0-12000 m altitude range. It is well known that the minimum voltage level at which corona discharges initiate decline with atmospheric pressure, i.e., at increasing altitudes. This is due to the fact that the mean free path of electrons increases when the air pressure decreases, so there are fewer collisions in the path of the electrons between the electrodes, but they are more energetic that at higher pressures, thus making the ionization process more effective [16].

2.3 Peek's law for visual corona

Peek's law [17] was derived more than a century ago using experimental data obtained from cylindrical conductors and it is widely accepted. It states that the visual electric field strength E_c at the surface of the conductor when visual corona effect starts can be expressed as,

$$E_c = E_0 m\delta\left(1+\frac{a}{\sqrt{\delta R}}\right) \quad [\mathrm{kV_{peak}/cm}] \qquad (1)$$

where E_0 [$\mathrm{kV_{peak}}$/cm] is the visual critical electric field strength measured at standard atmospheric conditions, a [$\mathrm{cm^{1/2}}$] is an empirical constant, R [cm] is the radius of the conductor, m is the roughness factor, and δ [-] is the relative air density, whose value depends on the atmospheric pressure. According to Peek, E_0 = 29.8 $\mathrm{kV_{peak}}$/cm and a = 0.301 $\mathrm{cm^{1/2}}$, under 50 Hz alternating current supply.

It is worth noting that the relative air density δ can be expressed as the ratio between the local and standard atmospheric pressures $\delta \approx k = P_{\mathrm{x\ kPa}}/P_{\mathrm{100\ kPa}}$, thus the pressure ratio k plays a key role in the strength of the visual critical electric field E_c.

In this experiment, the sizes of the spheres are small compared to the distance to the ground plate, so the equipotential curves adjacent to the sphere electrodes are nearly spherical in shape. Since the electric potential and field are related by $V = -\int E dr$, by integrating (1) in the surroundings of the boundary of the sphere and assuming m = 1 (we use perfectly polished bearing balls), it results the following expression of the corona visual voltage V_c,

$$V_c = E_0 kR\left(1+\frac{2a}{\sqrt{kR}}\right) \quad [\mathrm{kV_{peak}}] \qquad (2)$$

It is noted that (2) is not a conventional equation found in technical books, but an hypothesis that needs to be verified from experimental data. Rewriting (2), it leads to (3),

$$\frac{V_c}{kR} = E_0 + 2aE_0\frac{1}{\sqrt{kR}} \quad [\mathrm{kV_{peak}/cm}] \qquad (3)$$

According to (3), a linear fit of V_c/kR as function of $1/(kR)^{1/2}$ should yield the values for E_0 and a.

2.4 Paschen's law

It is well known that air density and atmospheric pressure have a strong influence on the dielectric properties of gases [18], and in particular on the voltages at which corona and complete breakdown occur. Paschen [19] carried out studies of gaseous spark gap breakdown in uniform fields generated between two parallel plate electrodes in different gases, including air at different pressures. Fig. 2 shows the Paschen's curve for air at 20 ºC based on the work of Dakin *et al.* [20].

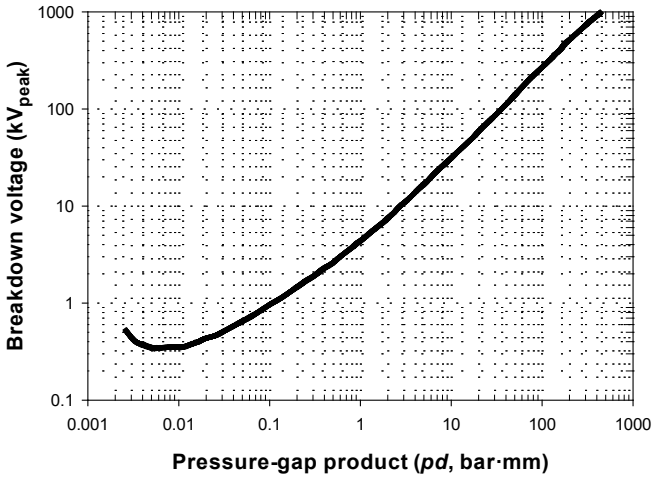

Fig. 2. Experimental Paschen curve for air at 20ºC adapted from [20,21], where d is the spacing between the electrodes and p is the pressure of air.

According to the Paschen's curve for air shown in Fig. 2, the breakdown voltage in uniform fields decreases when the pd product reduces, where p is the pressure of air and d is the

distance between the parallel plate electrodes. However, for very low pressure levels (relative vacuum conditions), the breakdown voltage increases when the *pd* product reduces. Therefore, Paschen's law states that the *pd* product of the pressure and a characteristic distance, in our experiment the *kR* product, determines the breakdown voltage. So the *kR* product is already present in Peek's law as observed in (1)-(3) and throughout the field of discharge physics.

3. Procedure to determine the CEV value

As detailed in the IEC 60270 standard [22], when gradually increasing the voltage from zero, the first point at which corona activity appears is known as corona inception voltage (CIV). However, when initiated, if the voltage is reduced, corona activity still can be observed until reaching a minimum voltage value known as corona extinction voltage (CEV), which is the lowest value of the voltage at which corona activity can be registered.

Fig. 3 shows the procedure applied to detect the CEV value under 50 Hz alternating current supply.

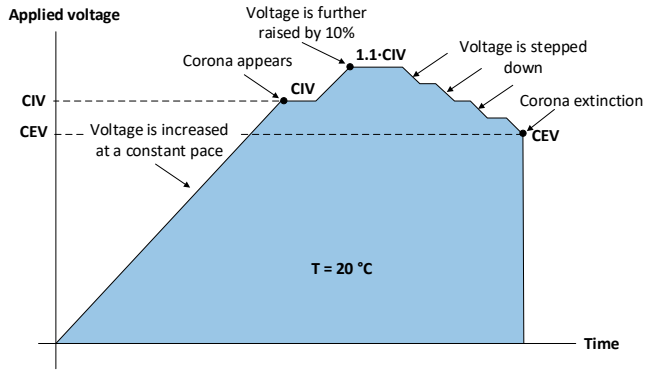

Fig. 3. Applied experimental method for determining the CEV value of the analysed sphere-to-plane air gaps.

4. Analysed electrodes and experimental setup

This section describes the samples analysed and the experimental setup.

4.1 Analysed Spherical Electrodes

The analysed sphere-to-plane gaps include a grounded square copper plate and stainless steel bearing balls of different diameters in the 2 – 10 mm range. They are mechanically and electrically connected to stainless steel tubes whose diameters are compressed in the 0.75 – 1.92 mm range, as shown in Fig. 4. The diameter of the tubes was carefully selected and matched with that of the spheres to minimize their influence. The lowest part of the sphere electrodes was placed 80 mm above the ground plane. Temperature was kept constant at 25 ºC during the experiments.

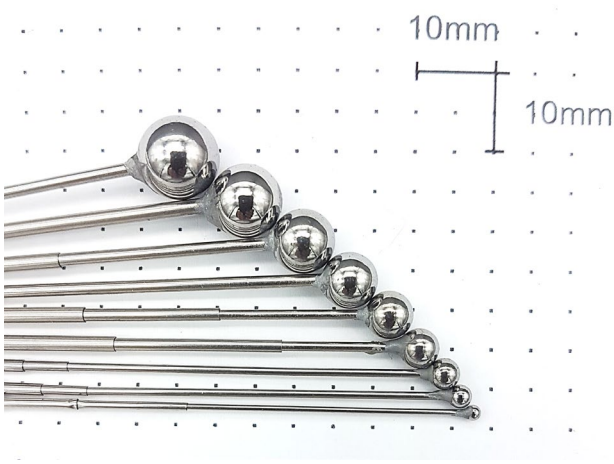

Fig. 4. Analysed spherical electrodes.

4.2 Experimental Setup

Corona tests performed in this work require a high voltage source. A low-voltage variable-amplitude ac source (APM Technologies SP300VAC600W, 0-300 V) was used to this end connected to a step-up high-voltage transformer (turns ratio 1:100, 36 kV maximum voltage, Laboratorio Electrotécnico). To measure the output voltage of the high-voltage transformer, a high-voltage probe (Testec TT-HVP40, voltage divider 1.000:1) was connected to a true-RMS voltmeter (Fluke 289).

Low-pressure experiments were performed in a low-pressure cylindrical chamber (diameter = 130 mm diameter and height = 375 mm) that incorporates a sealed lid and a hermetic pass through connector that allows passing thin wires from the inside to the outside of the low-pressure camera. The pressure was regulated using a vacuum pump (Bacoeng BA-1).

A gas-filled tube UV sensor (R9533-UVTRON, Hamamatsu) was used inside the low-pressure chamber to detect the corona discharges. This sensor is sensitive to the 185-265 nm range and uses the photoelectric effect of a metallic electrode and the gas multiplication of the electric current due to the electric discharge.

Fig. 5 shows a layout of the experimental setup.

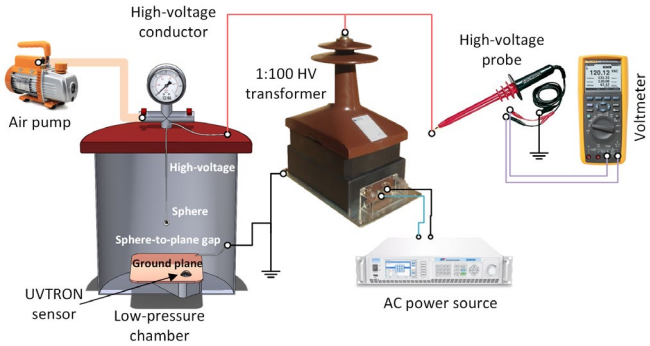

Fig. 5. Sketch of the experimental arrangement used in this work to detect the corona discharges at varying pressure conditions.

5. Results

This section presents and discusses the experimental values obtained in the laboratory. It is worth noting that further information and a more extensive data set can be found in a previous research paper of the authors [2].

First, to better understand how corona discharges look like, Fig. 6 shows long exposure photographs of such discharges taken with a high-resolution CMOS imaging sensor (Sony IMX586). In a previous work [23] the authors have shown that the energy contained in such photographs is proportional to the electric power dissipated by the discharges.

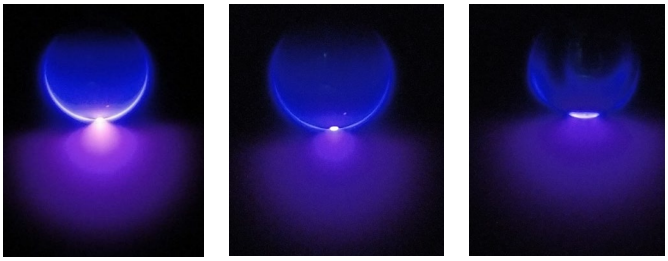

(a) (b) (c)

Fig. 6. Long exposure photographs of the corona discharges. (a) Corona photograph of the spherical electrodes used at 100 kPa, 28 kV. (b) Corona photograph of the spherical electrodes used at 60 kPa, 20 kV. (c) Corona photograph of the spherical electrodes used at 20 kPa, 8 kV.

5.1 Measured CEV values

Experimental results are presented in Table 2. CEV values were measured according to the procedure described in Fig. 3 using the experimental setup shown in Fig. 5.

Table 2. Summary of experimental values of the measured CEV values under 50 Hz alternating current supply

Air pressure (kPa)	Sphere diameter (mm)	CEV (Corona extinction voltage) (kV_{peak})
20	2	3.099
	3	3.901
	4	4.542
	5	5.055
	6	5.522
	7	6.371
	8	6.829
	9	7.154
	10	7.600
40	2	4.967
	3	6.280
	4	7.307
	5	8.508
	6	9.071
	7	10.519
	8	11.312
	9	12.117
	10	13.381
60	2	6.574
	3	8.285
	4	9.596
	5	11.241
	6	12.516
	7	13.961
	8	15.134
	9	16.180
	10	17.232
80	2	7.962
	3	10.129
	4	11.748
	5	13.843
	6	15.495
	7	17.001
	8	18.288
	9	19.665
	10	21.487
100	2	9.576
	3	11.972
	4	14.880
	5	16.731
	6	18.717
	7	19.913
	8	21.630
	9	23.467
	10	25.731

5.2 Validation of the Peek's law from experimental data

This subsection confirms the validity of Peek's law. The experimental values presented in Table 2 are arranged properly in Fig. 7, which plots $V_c/(kR)$ versus $(kR)^{-1/2}$ and the experimental fit according to (3), where V_c is the experimental CEV value. From this linear fit it results E_0 = 26.99 kV_{peak}/cm and a = 0.336 $cm^{-1/2}$ with a coefficient of determination R^2 = 0.9606. Note that the obtained values of E_0 and a are very close to the ones reported by Peek when analysing parallel cylindrical conductors, thus corroborating the applicability of Peek's equation.

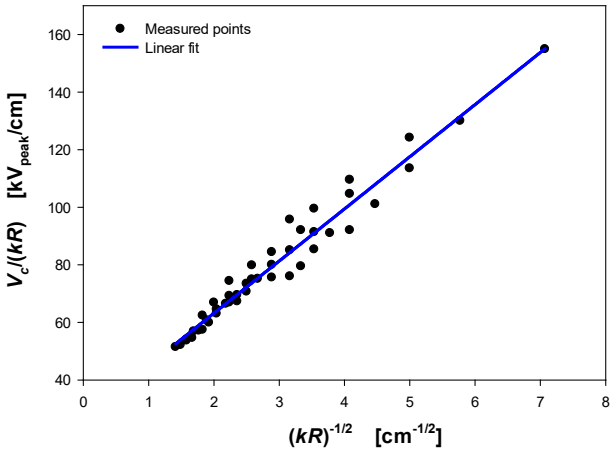

a)

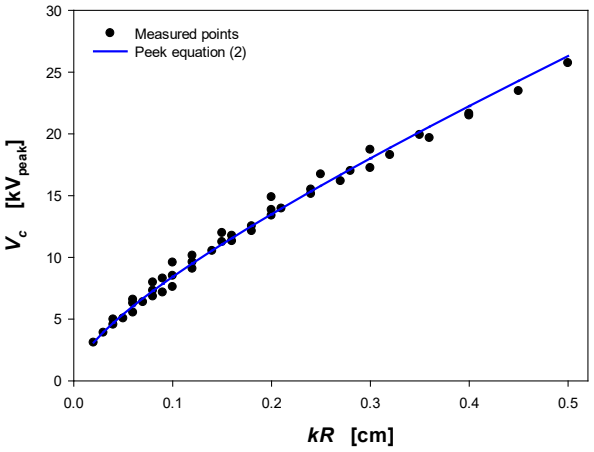

b)

Fig. 7. a) Experimental values from Table 2 plotted as $V_c/(kR)$ versus $(kR)^{-1/2}$ and the experimental fit according to equation (3), where V_c is the experimental CEV value. From the linear fit it results $E_0 = 26.99$ kV_{peak}/cm and $a = 0.336$ $cm^{-1/2}$. b) Experimental values of V_c versus kR and results of equation (2) versus kR using $E_0 = 26.99$ kV_{peak}/cm and $a = 0.336$ $cm^{-1/2}$.

Results presented in Fig. 7b show that all values in Table 2 (it considers different pressures) collapse onto a single curve, thus confirming Paschen's law and the correct shape of equation (2).

5.3 Influence of the radius and pressure on the CEV values

Fig. 8 shows a graphical visualization of the experimental CEV values presented in Table 2 as a function of the sphere diameter and atmospheric pressure.

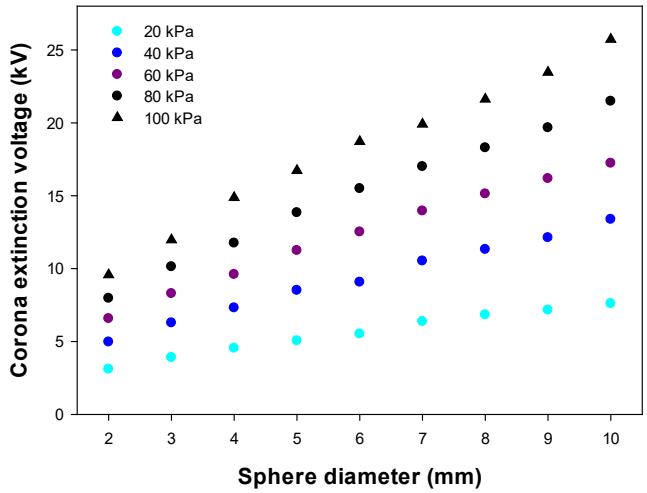

Fig. 8. Summary of the experimental CEV values obtained in the 20 – 100 kPa range using spherical electrodes in the 2 – 10 mm diameter range.

Results presented in Fig. 8 clearly show the key role of the diameter and pressure on the CEV values. Whereas the CEV value considerably increases with the diameter of the spherical electrode, it reduces with pressure.

Figs. 9 and 10 show these effects with more detail to better understand their role on the CEV value.

Fig. 9 shows the ratio between the CEV values measured at 80 – 60 – 40 – 20 kPa and the CEV values measured at 100 kPa, $CEV_{x\ kPa}/CEV_{100\ kPa}$ for the different spherical electrodes.

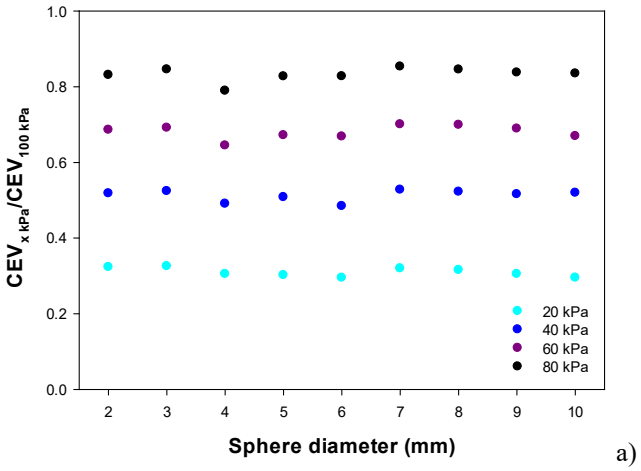

a)

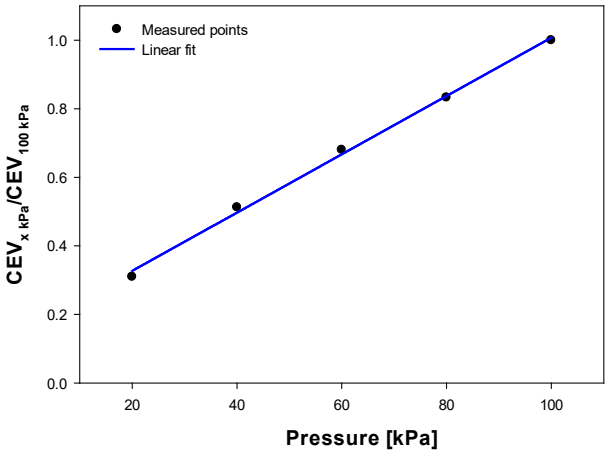

b)

Fig. 9. Pressure effect. a) Ratio between the CEV values measured at 80 – 60 – 40 – 20 kPa and the CEV values measured at 100 kPa for the different spherical electrodes. b) Average values of the $CEV_{x\ kPa}/CEV_{100\ kPa}$ as a function of pressure and its linear fit that results in a coefficient of determination $R^2 = 0.9973$.

Results presented in Fig. 9 clearly show the important effect of the atmospheric pressure on the CEV value. As expected, for a given pressure, the $CEV_{x\ kPa}/CEV_{100\ kPa}$ ratio is almost independent of the radius of the spherical electrode and it decreases linearly with the reduction of pressure.

Fig. 10 shows the effect of the electrode diameter for each pressure. It shows the ratio of the CEV values for 2–to–9 sphere diameters to the CEV values for the 10 mm sphere diameter at different pressures, $CEV_{x\ mm}/CEV_{10\ mm}$. As expected, when the diameter of the spherical electrode reduces, this ratio also reduces because CEV values decrease with the diameter of the electrode. Results in Fig. 10 also show that for a given pressure, the $CEV_{x\ mm}/CEV_{10\ mm}$ ratio is almost independent of the pressure. These results show the important role that the diameter plays on the CEV value.

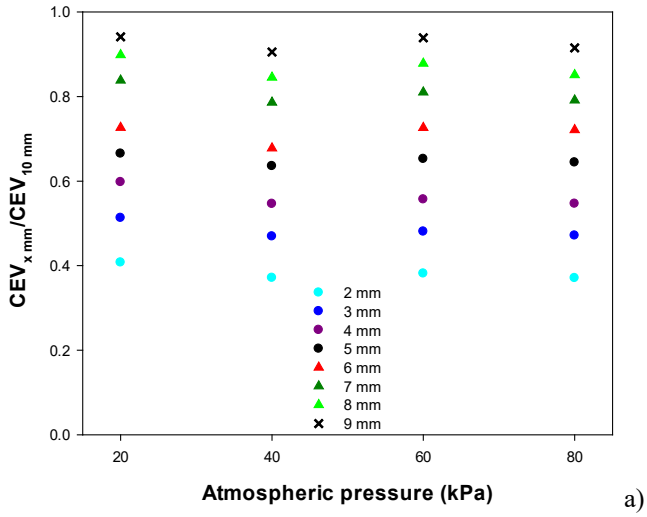

a)

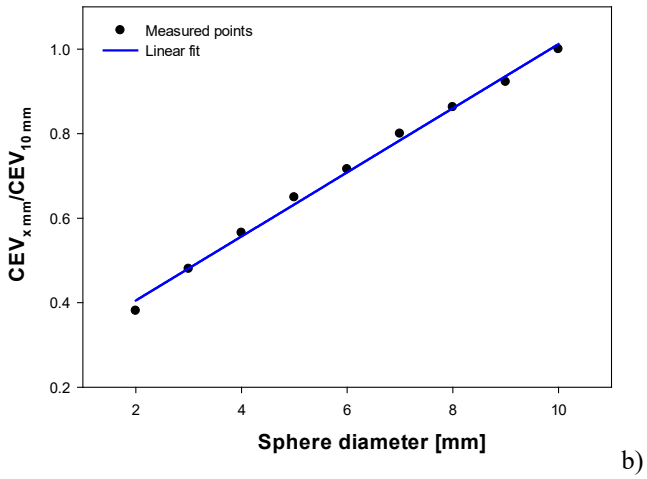

b)

Fig. 10. Geometry effect. a) Ratio of the CEV values for 2–to–9 sphere diameters to the CEV values for 10 mm sphere diameter at different pressures. b) Average values of the $CEV_{x\ mm}/CEV_{10\ mm}$ as a function of the sphere diameter and its linear fit that results in a coefficient of determination $R^2 = 0.9954$.

Results presented in Fig. 10 clearly show that the $CEV_{x\ mm}/CEV_{10\ mm}$ ratio is almost independent of the atmospheric pressure and decreases linearly with the reduction of the sphere radius.

6. Conclusion

In this work, the authors have proposed an experiment for undergraduate laboratories. It has introduced topics related to electrical discharges, that are suitable for students with intermediate physics knowledge. The experiments proposed in this paper can be applied for student projects or in practical sessions. Corona discharges are scarcely studied in regular physics courses despite their practical importance in different areas. This work has analysed the effect of geometry and atmospheric pressure on the corona extinction voltage (CEV) of spherical electrodes. The results presented clearly show that as the pressure and the diameter of the electrode decrease, CEV values also decrease.

We consider that the topics studied in this paper are worth for a students' project or a practical session for undergraduate laboratories, because they involve basic knowledge of electricity and fluids. The practical work could be oriented to study the combined effect of pressure and geometry on the minimum voltage at which corona discharges initiate, to analyse both effects separately or even to only study the effect of geometry.

Acknowledgements

This work was partially supported by Ministerio de Ciencia e Innovación de España, grant number PID2020-114240RB-I00 and by the Generalitat de Catalunya, grant number 2017 SGR 967.

References

[1] Ijumba N M, Lekganyane M J and Britten A C 2007 Comparative studies of DC corona losses in a corona cage and a point-plane gap *AFRICON 2007* (IEEE) pp 1–7

[2] Bas-Calopa P, Riba J-R and Moreno-Eguilaz M 2022 Measurement of Corona Discharges under Variable Geometry, Frequency and Pressure Environment *Sensors 2022, Vol. 22, Page 1856* **22** 1856

[3] Li Z-X, Li G-F, Fan J-B and Yin Y 2011 Numerical calculation of the corona onset voltage for bundle conductors for HVDC transmission line *Eur. Trans. Electr. Power* **21** 11–7

[4] Lu T, Xiong G, Cui X, Rao H and Wang Q 2011 Analysis of Corona Onset Electric Field Considering the Effect of Space Charges *IEEE Trans. Magn.* **47** 1390–3

[5] Chen J and Davidson J H 2003 Model of the Negative DC Corona Plasma: Comparison to the Positive DC Corona Plasma *Plasma Chem. Plasma Process.* **23** 83–102

[6] El-Bahy M M 2002 Onset voltage of negative corona in point-cup gaps *Annual Report Conference on Electrical Insulation and Dielectric Phenomena* (IEEE) pp 159–63

[7] Zhang Y, Liu L, Chen Y and Ouyang J 2015 Characteristics of ionic wind in needle-to-ring corona discharge *J. Electrostat.* **74** 15–20

[8] Goldman M and Sigmond R 1982 Corona and Insulation *IEEE Trans. Electr. Insul.* **EI-17** 90–105

[9] Wais S I and Giliyana D D 2013 Sphere-to-Plane Electrodes Configuration of Positive and Negative Plasma Corona Discharge *Am. J. Mod. Phys.* **2** 46–52

[10] Wang Z, Lu T, Cui X, Li X and Hiziroglu H 2016 Influence of AC voltage on the positive DC corona current pulses in a wire-cylinder gap View Documen *CSEE J. Power Energy Syst.* **2** 58–65

[11] Hernández-Guiteras J, Riba J-R and Casals-Torrens P 2013 Determination of the corona inception voltage in an extra high voltage substation connector *IEEE Trans. Dielectr. Electr. Insul.* **20** 82–8
[12] Riba J-R, Gomez-Pau A and Moreno-Eguilaz M 2020 Sensor Comparison for Corona Discharge Detection Under Low Pressure Conditions *IEEE Sens. J.* 1–1
[13] Riba J-R, Gómez-Pau Á and Moreno-Eguilaz M 2020 Experimental Study of Visual Corona under Aeronautic Pressure Conditions Using Low-Cost Imaging Sensors *Sensors* **20** 411
[14] Kuffel J, Zaengl W S and Kuffel P 2000 *High Voltage Engineering Fundamentals* (Oxford: Newnes)
[15] NASA 1976 U.S. Standard Atmosphere, 1976 1–242
[16] Riba J-R, Moreno-Eguilaz M, Ibrayemov T and Boizieau M 2022 Surface Discharges Performance of ETFE- and PTFE-Insulated Wires for Aircraft Applications *Mater. 2022, Vol. 15, Page 1677* **15** 1677
[17] Peek F W 1913 Law of Corona and Dielectric Strength of Air-III *Trans. Am. Inst. Electr. Eng.* **XXXII** 1767–85
[18] Eriksson A J, le Roux B C, Geldenhuys H J and Meal D V 1986 Study of airgap breakdown characteristics under ambient conditions of reduced air density *IEE Proc. A Phys. Sci. Meas. Instrumentation, Manag. Educ. Rev.* **133** 485
[19] Paschen F 1889 Ueber die zum Funkenübergang in Luft, Wasserstoff und Kohlensäure bei verschiedenen Drucken erforderliche Potentialdifferenz *Ann. Phys.* **273** 69–96
[20] Dakin T W, Luxa G, Oppermann G, Vigreux J, Wind G and Winkelnkemper H 1974 Breakdown of gases in uniform fields - Paschen's curves for air, N2 and SF6 *Elektra* **32** 61–82
[21] Husain E and Nema R S 1982 Analysis of Paschen Curves for air, N2 and SF6 Using the Townsend Breakdown Equation *IEEE Trans. Electr. Insul.* **EI-17** 350–3
[22] International Electrotechnical Commission 2000 *IEC 60270:2000 High-voltage test techniques - Partial discharge measurements* (International Electrotechnical Commission)
[23] Riba J-R, Gómez-Pau Á and Moreno-Eguilaz M 2020 Insulation Failure Quantification Based on the Energy of Digital Images Using Low-Cost Imaging Sensors *Sensors* **20**